Capillary instabilities in thin polymer films

Harkema, Stephan

Chapter 3

Experimental Techniques & Materials

3.1 Experimental set-up

A schematic representation of the experimental setup is shown in Fig.[3.1]. A typical set-up consists of a stack of 4 layers in the order: substrate, polymer, air and confining top surface. Several substrates were used, as is described in section 3.3.

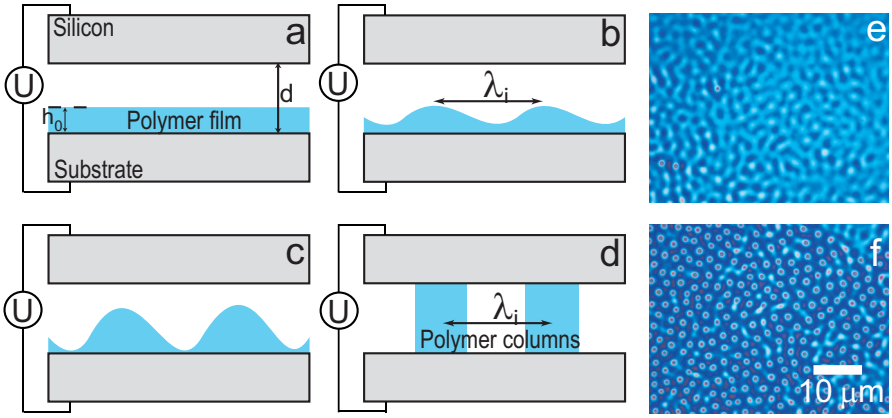

Figure 3.1: Schematic representation of the experimental set-up. a) A thin polymer film with initial film thickness h_0 is assembled between two parallel plates that are spaced apart by a distance d. With a voltage U applied, the polymer film destabilizes. In b), an instability forms throughout the film (see also e). The shape, characteristic for a spontaneously forming instability, is sinusoidal with a wavelength λ_i. With increasing amplitude of the film thickness variations, as visible in c), the film is pinned to the top wafer in d), thereby bridging the gap between the two plates (see also f).

Polymer films with thicknesses on the order of 100 nm were deposited on a solid substrate by spin-coating from a toluene solution containing 2-5% (by weight) polymer. Spin-coating is a well-know technique that is used for instance in the manufacturing of hard-disks, DVD's and in pattern replication techniques as photolithography, which is further described in section 3.5].

As the confining top surface, a single-sided highly polished silicon wafer was used. The surface of this wafer can either be flat or contain a patterned silicon structure, created by Electron Beam Writing (commercially obtained from X-lith eXtreme Lithography, Ulm, Germany). In both cases, the wafer was mounted onto the film with the polished side facing down, leaving an air gap $d - h$ on the order of $10^{-1}\,\mu$m.

The experiment was initiated by liquefying the polymer film while a voltage U was applied. Liquefying the film was accomplished either by 1) increasing the temperature of the assembly to well above the glass transition temperature of the polymer (typically to $\sim 170\,^{\circ}$C) or 2) by reducing the glass transition of the polymer to below room

temperature by exposing the polymer film to the vapor of a good solvent. Instead of a voltage, a temperature difference or surface charges on the top silicon wafer have also been used to induce structure formation in liquid polymer films. A setup similar to Fig.[3.1] was used in these experiments.

The assembly was left to anneal for several hours. The polymer structure that had formed during this period was frozen-in by reducing the temperature to room temperature or by removing the solvent vapor and allowing the film to dry.

To facilitate a non-destructive release of the confining surface after structure formation, the silicon wafer was rendered apolar by surface grafting of a self-assembled monolayer (section 3.6). The quenched polymer film was then characterized by optical microscopy (Olympus BX60) and by atomic force microscopy (AFM, Veeco Dimension 3100).

3.2 Polymers

The polymers were commercially obtained and used without further purification. Best suited for the experiments were linear homopolymers with a narrow molecular weight distribution $P_\mathrm{d} = M_\mathrm{w}/M_\mathrm{n}$. Primarily applied in the experiments described in this thesis are polystyrene (PS), polymethyl methacrylate (PMMA), brominated polystyrene ($\mathrm{PBrS_x}$, where x is the fraction of brominated monomers) and poly(vinyl methyl ether) (PVME). These polymers differ in an electric field or a temperature gradient by different values for properties, such as the dielectric constant ε, the velocity of sound v_p and the thermal conductivities.

Polymer	M_w (kg/mol)	P_d	γ (mN/m)[ϟ]	T_g (°C)	ε	n
PS[†‡]	22,94.9,100,515	<1.07	30.0	95–105	2.5	1.59
PBrS[‡]	154	1.02	≈30.0	135-140 [33]	5.5	2.4
PMMA[†‡]	100	1.07	30	105	3.6	1.49
PVME[§]	100	1.1	21	-40	2.5	1.52

Table 3.1: Polymers used in the experiments. M_w corresponds to the weight-averaged molecular weight, P_d to the polydispersity, γ to the surface tension of the polymer melt at 170°C, T_g to the glass transition temperature, ε to the dielectric constant and n to the refractive index at room temperature.

† *Polymer Standards Service GmbH, Mainz, Germany*

‡ *Fluka, Buchs, Switzerland*

§ *Polymer Source Inc., Dorval, Canada*

ϟ *CRC Handbook of Polymer Chemistry*

3.3 Substrates

As solid support for thin polymer films three substrates were used, all silicon based. Silicon is a metalloid (as opposed to metals and non-metals) that is produced from silica sand. It is the second most abundant element on earth (26%). On the atomic level, each silicon atom is covalently bonded to 4 other silicon atoms (tetravalent) in a 3-dimensional geometry (face-centered cubic lattice). To improve and tailor the electrical properties of the semiconducting silicon, atoms with a different number of valence electrons are inserted, such as boron (3 valence electrons) or phosphor (5 valence electrons).

In our experiments, we used p-doped silicon wafers (using boron as dopant) that have been cut across the <100> crystal plane. The wafers are highly polished and have a surface roughness below 5 nm. The silicon wafers were cleaned in a jet of CO_2 ice crystals (snow-jet) prior to spin-coating of the polymer thin film.

Wafer	Type	h	Ω	n
Si[†] <100>	p(B)	625±15 μm	7-13 Ω/cm^2	4.11
Si[‡] <100>	p(B)	625±25 μm	10-60 Ω/cm^2	4.11
Glass/ITO[§]	/	0.6 mm	80 Ω/cm^2	1.55
Glass/ITO	/	1.1 mm	155 Ω/cm^2	1.55

Table 3.2: Silicon based substrates used in the experiments
[†] *Wafernet Gmbh, Eching, Germany*
[‡] *UniversityWafers.com, South Boston, USA*
[§] *provided by the group of Paul Blom, University of Groningen*

Silicon, like other metalloids and metals, spontaneously forms a native oxide layer when exposed to oxygen. The native oxide layer of the silicon substrates used is approximately 2 nm thick. For experiments using uncompensated charges on a silicon oxide surface, isolating layers of silicon oxide were thermally grown at 950 °C on <100> p-doped silicon wafers. Charging of these layers was accomplished by snow-jet cleaning.

As transparent substrates, glass slides covered with a 105 nm thick layer of indium tin oxide were used. Indium tin oxide (ITO) is a transparent conductive material that consists of indium(III) oxide and tin(IV) oxide and allows (non-conductive) glass slides to be used while conductive and transparent substrates are required, like in electronic devices such as liquid crystal displays (LEDs), organic light emitting diodes (OLEDs) and in the electric field experiments described in this thesis. ITO covered glass slides with a resistance of 80 Ω cm^{-2} (substrate A) were used as substrates in addition to ITO covered glass with a resistance of 155 Ω cm^{-2} (substrate B). The glass slides (A) were cleaned by scrubbing with soap water at 75 °C, washed in an ultrasonic bath with acetone and propan-2-ol, consecutively, and finally irradiated for 20–30 minutes

in an UV-ozone cleaner. The glass slides (B) were cleaned by snow-jet cleaning (CO_2 crystals) prior to film deposition.

3.4 Snow-jet cleaning

Snow-jet cleaning is a single-step and environmentally friendly cleaning procedure using a jet of carbon dioxide ("snow-jet"). The expansion of high pressure carbon dioxide is guided through a nozzle and aimed at a solid surface. Snow cleaning was first shown by Hoenig in 1986[17] for low velocity gas streams, later by Whitlock in 1989[40] for high velocity gas streams.

Two complementary mechanisms were proposed by Whitlock in 1989. By itself, the aerodynamic drag exerted by a gas stream on adhered particles is insufficient. However, in the expanding high velocity carbon dioxide gas stream, the pressure and the temperature drop. This nucleates the formation of ice crystals in a humid atmosphere. On impact, the carbon dioxide and ice crystals provide sufficient momentum to remove sub-micron and micron sized particles that have adhered to the surface.

The second mechanism involves solvent action from liquefied carbon dioxide. Due to an increased pressure on impact with the solid surface, the carbon dioxide crystals liquefy and act as solvent for chemical heterogeneities. Upon rebound and solidification of CO_2, the high-velocity stream carries away the newly formed particles containing the chemical contaminations with efficiencies up to 99.99%[30].

The original technique, snow cleaning, has been supplemented with LCO_2 (liquid carbon dioxide) cleaning, CO_2 pellet cleaning and $SCCO_2$ (super critical carbon dioxide) cleaning. With an improved solvency and penetrating power, $SCCO_2$ cleans a wider range of contamination, even down to the atomic level.

3.5 Spin-coating

Thin organic films can be deposited onto a surface using various techniques, such as dip coating, spray coating, flow coating, capillary coating, roll coating, electrocoating, chemical coating, printing, and so on. The films that were used in the experiments that are described in this thesis were obtained by spin-coating from a toluene solution (2-5% by weight).

Spin-coating is a straight-forward process to coat a flat substrate with a thin film using a centrifugal force. This is achieved by wetting a substrate with a solution and subsequently rotating the substrate at a speed in the order of 10^3 rotations per minute. Since 1922, a spinning disc has been employed to prepare thin homogenous films, for instance of paints and varnishes[38]. The mechanism of a flow of a viscous liquid on a rotating disc was first described by Emslie, Bonner, and Peck in 1958[13].

The spin coating process consists of four stages. In the first stage, a solution containing several % (by weight) of polymer is deposited onto the substrate. To

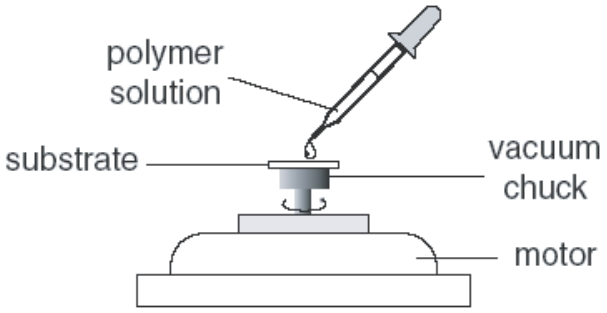

Figure 3.2: Schematic representation of the spin-coating technique. Used with permission, courtesy of Mihai D. Morariu.

obtain a smooth and defect-free film, a filtered solution (filter pore size of 100 nm) is used that wets the substrate. In the second stage, the substrate is accelerated towards the final rotating speed. During the acceleration, excess solution on the substrate is expelled. In the third stage, the substrate is spinning at constant rotation speed, covered by a thinning viscous solution. The gradual and uniform drying of the film in this stage is dominated by the viscous forces. In the last stage, the evaporation of the solvent from the film is dominant. With sufficient reduction of solvent in the film, a glassy and homogenously flat coating is obtained.

The competition between the centrifugal force and the evaporation rate of the solvent determines the film thickness of the dry film. Both viscosity and density increase as evaporation progresses during spinning of the solution. Emslie *et al.*[13] assumed a balance of viscous and centrifugal forces and based on this assumption they predicted the final film thickness. In this model, the effects of inertia in the initial stage of spinning and the non-Newtonian flow effects at high shear were not included[7,25]. Meyerhofer[22] assumed that the early stages were entirely dominated by the flow characteristics, while later stages would be entirely dominated by solvent evaporation. He included the evaporation rate in the final coating thickness by assuming that evaporation at constant rotation rate remains constant throughout spinning. Sukanek included an evaporation rate that depended on the average solvent concentration in the film[36], as well as a non-Newtonian behavior[37] of the drying film.

3.6 Surface energy modification

To facilitate the removal of the confining silicon surface (see Fig.[3.1]), the silicon surface was rendered apolar (low surface energy) in order to reduce adhesion of the

polymer to the silicon surface. This was accomplished by the physisorption of a silicon based compound with a long alkane chain (octadecyltrichlorosilane, OTS) from solution. This chemical reaction, called silanization, was first applied by Sagiv[29] on oxidized silicon wafers, and was based on the deposition from solution technique by Bigelow, Pickett and Zisman[3]. OTS forms covalent bonds with the oxygen groups on a (native) silicon oxide surface and self-assembles into a highly-ordered monolayer[8,29,31,39].

In our silanization procedure, the silicon surface was cleaned by snow-jet cleaning and placed in a reactive etching solution, Piranha, for 30 minutes at 80 °C. Piranha is a solution that contains the oxidant peroxydisulfuric acid (PSDA). PSDA is formed when hydrogen peroxide and sulfuric acid are mixed. In a 3:1 (v/v) ratio of 98% sulfuric acid and 30% H_2O_2, chemical contaminants were readily oxidized and after extensive rinsing in Millipore water and drying in a stream of dry N_2 gas, silicon surface with a high surface energy was obtained.

Silanization was performed by immersing the freshly cleaned silicon wafer in a glass beaker containing 50 ml of hexadecane with 10-20 drops of OTS and 5-10 drops of tetrachloromethane (CCl_4). To prevent a premature reaction of the OTS with moisture from the atmosphere, the humidity of the reaction vessel was reduced by a continuous flow of dry nitrogen. The substrate was left to react during 4-5 hours, followed by washing in tetrachloromethane and chloroform. After drying in dry nitrogen gas, water contact angles, typically above 90 ° (lit. 110 °[29,39]) were obtained, sufficiently high for our purposes.

3.7 Thermal Annealing & Vapor Sorption Annealing

The liquefaction of polymer films at room temperature (despite a glass transition temperature far above room temperature) is possible by absorption of solvent vapor[9,10,21]. The softening of a glassy polymer by the absorption of solvent vapor was introduced in the experiments described in this thesis as an alternative to thermal annealing of a polymer film (Chapters 7, 9 and 10). Following liquefaction of the polymer, an electric field was applied, thereby inducing an instability that led to the destabilization and rupture of the polymer film.

It is known for many years that the free volume in a polymer is increased by raising the temperature or adding a low molecular weight material[15]. The absorption of gasses from our atmosphere such as carbon dioxide and exhaust fumes into polymers has great implications for the material properties of these polymers. The changes in thermal and mechanical properties caused by the absorption of gasses has become a valuable technique to manipulate the mechanical properties of polymers. In a controlled fashion, the absorption of gasses and liquids into polymers has found many scientific and technological applications in areas, such as food engineering[32], plastic recycling, but also photolithography[18], membrane science[20], biomedical engineering[23]

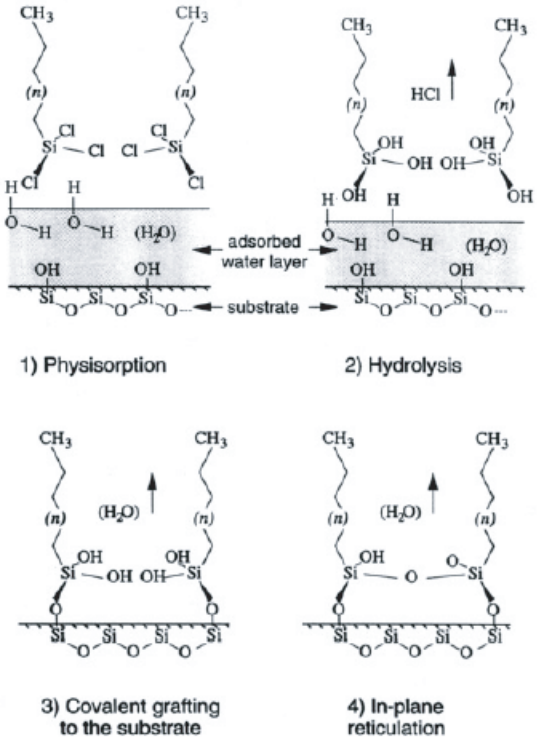

Figure 3.3: General scheme proposed by Brzoska et al. for the silanization reaction[8]*. Reprinted with permission from J.B. Brzoska, I.B. Azouz, and F. Rondelez, Langmuir, 1994, 10, 4367-4373. Copyright (1994), American Chemical Society.*

and high-pressure rheology[27].

Liquid mixtures of two components with different surface tensions show a segregation of the low surface tension component at the interfaces[2,28]. This applies to blends of homopolymers, homopolymer blockcopolymer blends, metal alloys, but has also been observed for several polymer/solvent systems[2]. Surface enrichment occurs not only at the liquid/air interface, but also at the substrate interface, with consequences for the stability of thin blend films[14]. In Chapter 4, the decreased stability and subsequent dewetting of a polymer system that shows surface enrichment, namely PS/PVME blends, is described.

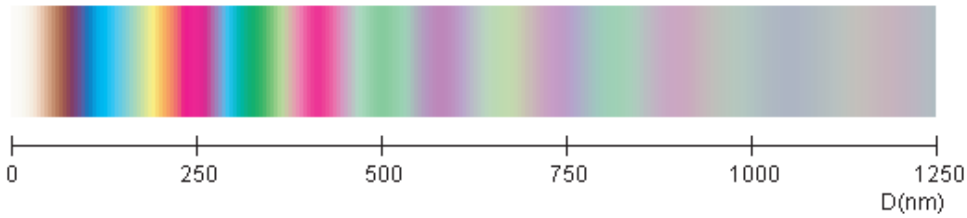

Figure 3.4: Interference of white light in a thin film. The color spectrum was approximated using the Java applet provided by Winston Chan while at the University of Iowa. (see http://home3.netcarrier.com/∼chan/EM/PROGRAMS/THINFILM/)

3.8 Optical Microscopy on thin polymer films

Since the invention of the microscope in the early 17^{th} century by the Janssen brothers and Galileo, the microscope has become an important research tool in many sciences, such as physics, materials sciences, life sciences, biology, forensics, biomedics and for the semiconductor industry.

In the simplest of definitions, a microscope is designed to produce a magnified image of an object that is too small to be seen with the naked eye. In addition to the magnification of small objects, sufficient contrast between separate objects and/or the background has to exist. In the conventional brightfield microscopy, objects with a similar refractive index as their background, hardly show any contrast and are thus barely distinguishable. To improve the contrast, several other techniques can be employed, such as darkfield (or darkground) illumination, polarization of light, fluorescence, phase contrast imaging, and many more.

To qualitatively analyze structure formation in polymer films, we have used brightfield reflection microscopy (Olympus Optical Microscopes GX61 and BX40). Features ranging from 10^{-6} m to 10^{-3} m have been observed by the reflection of white light from of the sample. By visual perception through the objective and subsequent (time-lapsed) digital recording of the observed features, using a digital camera and imaging software (Carl Zeiss Visiocam), we complement our data of *ex post facto* micrographs with *in-situ* recordings of structure formation in thin polymer films.

The colors in the images that are shown in this thesis[1] are not digitally improved. The constructive interference of white light with thin films and the surfaces they cover provides the appearance of color. The color of the film is a function of the thickness of the film, the refractive indices of the film, the substrate and the atmosphere. The color of a film can therefore be used as an indication of its thickness. These interference

[1]This thesis is also available in full color on the website of the Library of the University of Groningen: http://dissertations.ub.rug.nl/

colors, shown in Fig.3.4, make the perception with optical microscopy of small features and thickness variations in thin polymer films of several nm and larger much more straightforward.

3.9 Atomic Force Microscopy

Atomic Force Microscopy[6] is based on Scanning Tunneling Microscopy[5], an invention by Binnig and Rohrer, who were awarded the Nobel Prize in Physics in 1986.

In Scanning Tunneling Microscopy (STM), a conductive sample surface is investigated by measuring the tunneling of electrons from the surface atoms to the tip of an ultrasharp electrode[4,5]. To overcome the restriction of STM of only being applicable to conductive surfaces, the technique was extended. By measuring forces between a probe and a surface, also non-conductive materials could be imaged. This technique, called Atomic Force Microscopy, was invented by Binnig, Quate and Gerber[6] and has become a widely used high resolution imaging tool.

The challenge of the past decades has been the observation of subatomic length scales by AFM. Following the invention of STM, a 7x7 unit cell of Si with a <111> crystal orientation was observed and reported[5]. Atomic resolution with AFM was shown for $CaCO_3$ in water 1993[24], but the experimental results were considered controversial. Atomic defects were not visible and the recorded images could not be reproduced by theoretical models. In the theoretical[19,34] and experimental[16,34] studies that followed, evidence that supported the claims of atomic resolution mounted, thereby demonstrating the potential of Atomic Force Microscopy.

In Atomic Force Microscopy, the force experienced by the attraction and repulsion of the AFM probe (a cantilever with sharp tip) while in proximity to a surface is monitored and readjusted to a fixed set point. During line-by-line movement across the sample, the tip follows the contours of the surface while the force is kept constant. In addition to the short-ranged molecular forces that are measured with an ultra-sharp tip, the tip also experiences meniscus forces caused by capillary condensation. Capillary condensation occurs when a curved tip is held in proximity (up to $\approx 20\,\mathrm{nm}$)[35] to a surface. The relative humidity and the curvature of the tip play an important role in the formation of the water film in between the tip and the surface. Altering the tip characteristics, such as the radius, the surface energy and the material, allows a wider range of interactions to be investigated, from short-range molecular[35] to long-range electrostatic forces[12].

Because the force that is experienced by the tip is held constant, the distance between the sample and tip is effectively held constant. During scanning, the tip follows the contours of the sample topography faithfully. This control is achieved by a laser beam that is reflected from the cantilever and detected by a position sensitive photodiode. The position of the laser reflection on the diode, and thus the vertical displacement of the cantilever, is the input of an electrical circuit containing

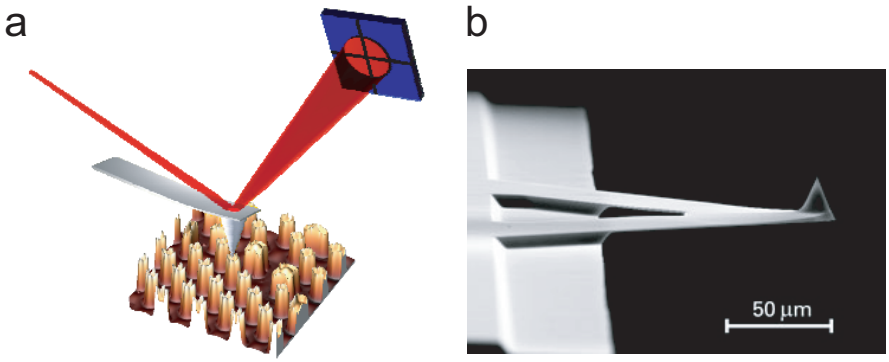

Figure 3.5: Atomic Force Microscopy: A laser is reflected from a cantilever containing a sharp tip. The surface induced bending of the cantilever causes the reflection to move vertically or horizontally on the detector. Using a feedback loop, the force or distance of the tip to the surface is held constant. The image on the right shows an electron micrograph of a triangular cantilever[2]. On top of the cantilever, the sharp tip used for imaging is shown. The electron micrograph is used with permission, courtesy of MikroMasch (http://www.spmtips.com/).

a feedback loop. The feedback electronics maintains a constant tip-sample distance by realigning the sample, in x, y and z-direction and thereby correcting any changes in the tip-sample separation. This is accomplished by altering the voltages applied to piezoelectric ceramics onto which the cantilever (or the sample) is mounted. The applied electric field deforms the piezoelectric material, thereby moving the cantilever (or sample) in a direction of choice. The voltage that is required to keep the tip-surface distance constant is interpreted by software to produce and display the topography of the sample surface.

Several scanning modes can be employed to probe a sample surface. The mode used to analyze the polymer structures in this thesis is called tapping or intermittent contact mode. Here, the cantilever oscillates just below its resonance frequency (150-300 kHz) with an amplitude on the order of 10 nm. In contrast to the contact mode, the tip only briefly comes into contact with the surface, thereby reducing the damage done to the sample surface during scanning. In proximity to the surface, the forces on the tip influence the frequency, amplitude or phase of the oscillation. In addition to topographic information, the interaction of the tapping tip and the surface also provides information on the mechanical properties of the surface material.

3.10 Ellipsometry

Ellipsometry is a non-destructive optical technique that relates changes in polarization of monochromatic (single wavelength) light upon reflection to the optical properties of surfaces and coatings it was reflected from[11,26,41]. Some of the surface properties that may be determined are layer thickness (for one or more films), refractive index, morphology, chemical composition and roughness.

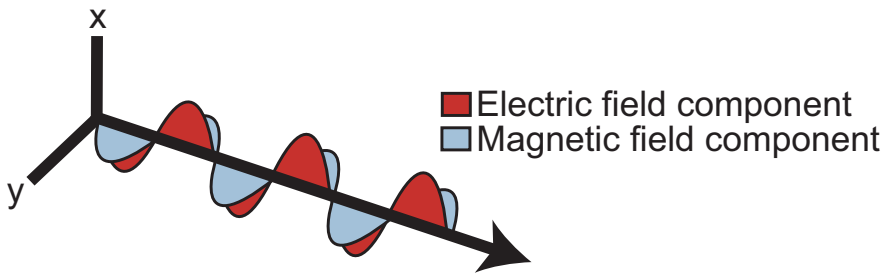

Figure 3.6: Oscillating electric and magnetic field components of light.

Light, as other electromagnetic radiation, has an oscillating electric field and a magnetic field component. In the direction of light wave propagation, both fields are sinusoidal in shape. Their field vectors are directed perpendicular with respect to each other and to the direction of propagation (Fig.[3.6]). Usually, only the electric field component is considered. In any reference frame, the electric field can be split into two vectors, one along the x-axis and one along the y-axis (Fig.[3.7]). With respect to a sample surface, the electric field vectors along the x- and y-axis can therefore be described in terms of components that are parallel and perpendicular to the plane of incidence, indicated by E_p and E_s, respectively. Depending on the amplitude of the electric field vectors and the phase difference between them, the light is either linearly (a), circularly (b) or elliptically (c) polarized. Polarizers, such as a Polaroid filter, can be used to change the polarization of light by absorbing light oscillations in one direction (anisotropic transmission), thereby transforming circularly or elliptically polarized light into linearly polarized light.

When light is anisotropically reflected off a surface, the polarization of light changes as a function of the angle of incidence, the angles of reflection, and the refractive indices of the materials. In null ellipsometry, the method used in this thesis, a single wavelength laser is linearly polarized using a polarizer (P). The axis of the polarizer determines the angle of polarization. The linearly polarized light is then circularly polarized by the quarter-wave plate (also known as the retarder or compensator C) that induces a phase shift of 90 °. Upon reflection from the sample surface, the size and shape of the ellipse of polarization is changed from b) to c) in

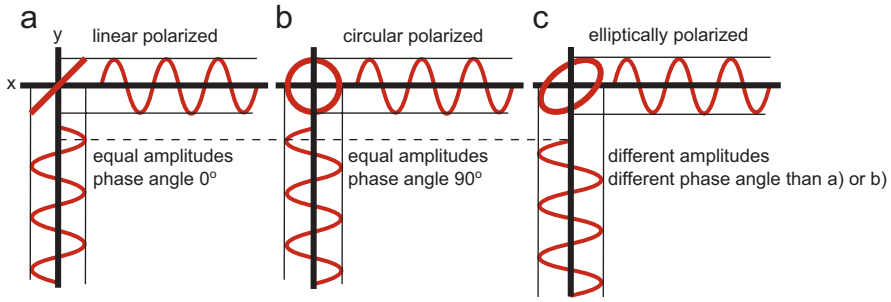

Figure 3.7: Polarization of the electric field component as a function of the amplitude and phase angle between the two electric field vectors. a) linear polarization: the amplitudes are equal and the phase angle is 0°, b) circular polarization: like a), but the phase angle is 90°, c) elliptically polarized: dissimilar amplitudes and a phase angle between the vectors $\neq n\pi$*, where* $n = \pm 0, 1, 2$.

Fig.[3.7]). The analyzer (A) is quite similar to the polarizer and only allows light that is polarized along its axis to reach the detector. The photo-detector measures the intensity of polarized light and at nulling conditions, that is achieved for for a specific set of angles for P, C and A, a minimum intensity is detected.

The theory of ellipsometry is based on the Fresnel reflection or transmission equations for polarized light encountering interfaces in planar multi-layered materials[1](Eq.[3.1]-Eq.[3.3]).

$$\rho = \frac{R_{\mathrm{p}}}{R_{\mathrm{s}}} = \tan \Psi e^{i\Delta} \tag{3.1}$$

$$R_p = \frac{n_1 \cos(\theta_1) - n_2 \cos(\theta_2)}{n_1 \cos(\theta_1) + n_2 \cos(\theta_2)} \tag{3.2}$$

$$R_s = \frac{n_1 \cos(\theta_2) - n_2 \cos(\theta_1)}{n_1 \cos(\theta_2) + n_2 \cos(\theta_1)} \tag{3.3}$$

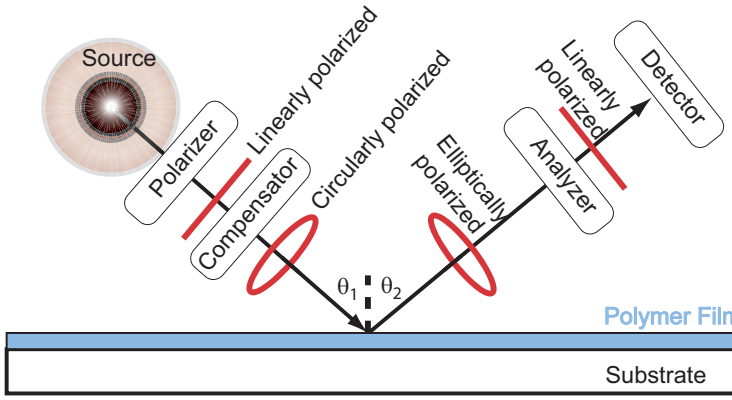

Figure 3.8: Schematic representation of a null ellipsometer. Monochromatic light from the laser source S passes through the polarizer P and compensator C and impinges onto the sample surface at incident angle θ_1. Upon reflection under the angle $\theta_2 = \theta_1$, the polarization has changed from circular to elliptical. Light polarized along the axis of analyzer A is detected by a photo-detector D. For a setting of P, C in a way that the reflected light is linearly polarized, a minimum (null) intensity is detected for a setting of A perpendicular to the polarization direction of the reflected light.

The Fresnel equations relate the experimentally determined reflection coefficients in the parallel direction (R_p) and in perpendicular direction (R_s) to the relative amplitude diminution ($\tan(\Psi)$) and the relative phase retardation (Δ). In Eq.[3.1]-Eq.[3.3], the light has an angle of incidence given by θ_1, an angle of reflection $\theta_2 = \theta_1$ and the refractive indices of the ambient atmosphere and surface coating, given by n_1 and n_2, respectively. The ellipsometric angles Ψ and Δ are a function of the angles obtained for the polarizer, analyzer and compensator. The thickness of the coating and the complex refractive index are obtained by comparing the ellipsometric angles to a theoretical model of the given experimental system. The ellipsometer used to characterize the polymer films in our experiments is an EP^3-SW single wavelength imaging ellipsometer (Nanofilm, Germany) with a lateral resolution of 1 μm.

Bibliography

1. R. M. A. Azzam, and N. M. Bashara,
Ellipsometry and Polarized Light, North Holland Press, Amsterdam, 1977, 2nd Ed.

2. Q.S. Bhatia, D.H. Pan, and J.T. Koberstein,
Macromolecules, **1988**, 21, *2166*

3. W.C. Bigelow, D.L. Pickett, and W.A. Zisman,
J. Colloid Sci., **1946**, 1, *513*

4. G. Binnig, H. Rohrer, Ch. Gerber, and E. Weibel,
Phys. Rev. Lett., **1982**, 49, *57*

5. G. Binnig, H. Rohrer, Ch. Gerber, and E. Weibel,
Phys. Rev. Lett., **1983**, 50, *120*

6. G. Binning, C.F. Quate, and Ch. Gerber,
Phys. Rev. Lett., **1986**, 56, *930*

7. J.A. Britten, and I.M. Thomas,
J. Appl. Phys., **1992**, 71, *972*

8. J.-B. Brzoska, I.Ben Azouz, and F. Rondelez
Langmuir, **1994**, 10, *4367*

9. T.S. Chow,
Macromolecules, **1980**, 13, *362*

10. E.A. DiMarzio, and J.H. Gibbs,
J. Pol. Sci.: A, **1963**, 1, *1417*

11. P. Drude,
Ann. Physik Chemie, **1890**, 39, *481*

12. W.A. Ducker, T.J. Senden, and R.M. Pashley,
Nature, **1991**, 353, *239*

13. A.G. Emslie, F.T. Bonner, and L.G. Peck,
J. Appl. Phys., **1958**, 29, *858*

14. B.D. Ermi, A. Karim, and J.F. Douglas,
J. Pol. Sci.: Part B: Pol. Phys., **1998**, 36, *191*

15. J.D. Ferry,
Viscoelastic Properties of Polymers, **1970**, John Wiley and Sons, NY, 2nd Ed.

16. F.J. Giessibl, S. Hembacher, H. Bielefeldt, and J. Mannhart,
Science, **2000**, 289, *422*

17. S.A. Hoening,
Compressed Gas Magazine, **1986**

18. E.N. Hoggan, K. Wang, D. Flowers, J.M. DeSimone, and R.G. Carbonell,
IEEE Trans. Semicond. Manuf., **2004**, 17, *510*

19. M. Huang, M. Cuma, and F. Liu,
Phys. Rev. Lett., **2003**, 90, *256101*

20. N.H. Jalani, P. Choi, and R. Datta,
Solid State Ionics, **2004**, 175, *815*

21. A. Laschitsch, C. Bouchard, J. Habicht, M. Schimmel, J. Rühe, and D. Johannsmann
Macromolecules, **1999**, 32, *1244*

22. D. Meyerhofer,
J. Appl. Phys., **1958**, 49, *3993*

23. B. Narasimhan,
Adv. Drug Deliv. Rev., **2001**, 48, *195*

24. F. Ohnesorge, and G. Binnig,
Science, **1993**, 260, *1451*

25. T.J. Rehg, and B.G. Higgins,
Phys. Fluids, **1988**, 31, *1360*

26. A. Rothen,
Rev. Sci. Instrum., **1945**, 16, *26*

27. J.R. Royer, Y.J. Gay, J.M. DeSimone and S.A. Khan,
J. Polymer Science, **2000**, 38, *3168*

28. T.P. Russell,
Ann. Rev. Mat. Sci., **1991**, 21, *249*

29. J. Sagiv,
J. Am. Chem. Soc., **1980**, 102, *92*

30. R. Sherman, D. Hirt, and R. Vane,
J. Vac. Sci. Technol. A, **1994**, 12, *1876*

31. P. Silberzan, J.L. Léger, D. Ausserré, and J.J. Benattar,
Langmuir, **1991**, 7, *1647*

32. P.P. Singh, D.E. Maier, J.H. Cushman, K. Haghighi, and C. Corvalan,
J. Math. Biol., **2004**, 49, *1*

33. D. Slep, J. Asselta, M.H. Rafailovich, J. Sokolov, D.A. Winesett, A.P. Smith, H. Ade,Y. Strzhemechny, S.A. Schwarz, and B.B. Sauer,
Langmuir, **1998**, 14, *4860*

34. I. Yu. Sokolov, G.S. Henderson, and F.J. Wicks,
J. Appl. Phys., **1999**, 86, *5537*

35. T. Stifter, O. Marti, and B. Bhushan,
Phys. Rev. B., 2000, 62, 13 667

36. P.C. Sukanek,
J. Imag. Tech., **1985**, 11, *184*

37. P.C. Sukanek,
J. Electrochem. Soc, **1991**, 138, *1712*

38. P.H. Walker, and J.G. Thompson,
Proc. Am. Soc. Testing Materials, **1922**, 22 (II), *464*

39. S.R. Wasserman, Y.-T. Tao, and G.M. Whitesides,
Langmuir, **1989**, 5, *1074*

40. W.H. Whitlock,
Proceedings of the 20th Annual Meeting of the Fine Particle Society, **1989**

41. A.B. Winterbottom,
Trans. Faraday Soc., **1946**, 42, *487*